Advances in Water Resources 146 (2020) 103789

Contents lists available at ScienceDirect

Advances in Water Resources

journal homepage: www.elsevier.com/locate/advwatres

Characterization of the micro-scale surface roughness effect on immiscible fluids and interfacial areas in porous media using the measurements of interfacial partitioning tracer tests

Hao Jiang[a], Bo Guo[b], Mark L. Brusseau[b,c,*]

[a] Department of Chemical and Environmental Engineering, University of Arizona, 1133 E James E Rogers Way, Tucson, AZ 85721, United States
[b] Department of Hydrology and Atmospheric Sciences, University of Arizona, 1133 E James E Rogers Way, Tucson, AZ 85721, United States
[c] Department of Environmental Science, University of Arizona, 429 Shantz Bldg., Tucson, AZ 85721, United States

ARTICLE INFO

Keywords:
Interfacial area
Surface roughness
Wetting film
Water adsorption
And capillarity

ABSTRACT

This study presents a model-based methodology to characterize the surface roughness effect on immiscible fluids in porous media using the measurements obtained with the gas-phase interfacial partitioning tracer test (IPTT). The characterization approach captures how adsorbed wetting film configuration on grain surfaces influences fluid-fluid interfaces in unsaturated porous media. The method establishes a novel representation of surface and interface roughness that delineates the micro-scale fractal nature of grain surfaces and the fluid-surface interactions at these scales. The method was tested using reported experimental data for several soils. The results showed that the methodology was effective for natural porous media comprising a range of physical and geochemical properties. Comparisons between characterized parameters of different media revealed that micro-scale surface roughness was only partially correlated to soil texture properties. Images of the test media obtained with scanning electron microscopy (SEM) illustrates the complexity of micro-scale surface roughness, and its variability among different media. Tests with an organic liquid–water system validated the generalness of surface roughness properties generated by the model. The proposed methodology is anticipated to provide a means to characterize and quantify the effects of surface roughness on fluid-solid interaction and fluid-fluid interfacial area, which are critical to various environmental disciplines.

1. Introduction

The interactions between immiscible fluids and rough solid surfaces play a significant role in various soil and hydraulic properties and in mediating mass and energy transfer. It has been shown that surface roughness has significant impacts on the wettability of solid surfaces (e.g., Wenzel, 1936; Cassie and Baxter, 1944; Hirasaki, 1991; Oliver et al., 1980), which is closely associated with the configuration of fluids in soil. It has also been demonstrated that surface roughness can influence the resistance of flow over fractured surfaces in unsaturated media (e.g., Brown, 1987; Lampurlanés and Cantero-Martínez, 2006; Or and Tuller, 2000; Thompson and Brown, 1991; Tokunaga and Wan, 1997), which is a critical factor for the hydraulic conductivity of a medium. Wetting-fluid configuration on rough surfaces can also influence both film interfacial area and film thickness (e.g., Kim et al., 2012; Tokunaga, 2011; Zheng et al., 2015; Jiang et al., 2020). Thus, potential relationships between surface roughness and other fluid and flow properties are of interest for numerous applications.

The complex nature of surface roughness poses challenges to develop a universal fluid-surface function for the great variety of natural porous media. Typically, surface roughness can be defined from three different viewpoints (e.g., Ghanbarian et al., 2016; Wenzel, 1936), each of which represents a specific principle for the interactions with fluids. The three approaches are conceptualized in the left column of Fig. 1.

The traditional definition of surface roughness is based on the average value of measured vertical coordinates compared to a reference level (relative surface height), e.g., arithmetic roughness (R_a) or root-mean-square roughness (R_{rms}). However, the relative surface height definition was found insufficient in practice due to the lack of consideration of fractal topology (Brown, 1987, 1989; Ghanbarian et al., 2016). The second definition of surface roughness originates from the basic concept of fractal geometry (Mandelbrot, 1983), in which either the pore surfaces (2D) or the entire porous medium (3D) are modified with corrections of fractal dimension, resulting in higher dimensions for surfaces (Brown, 1987; Ghanbarian et al., 2016) or lower dimensions for entire media (Crawford, 1994; Giménez et al., 1997; Toledo et al., 1990). It is

* Corresponding author.
E-mail address: brusseau@email.arizona.edu (M.L. Brusseau).

https://doi.org/10.1016/j.advwatres.2020.103789
Received 22 January 2020; Received in revised form 6 August 2020; Accepted 8 October 2020
Available online 9 October 2020
0309-1708/© 2020 Elsevier Ltd. All rights reserved.

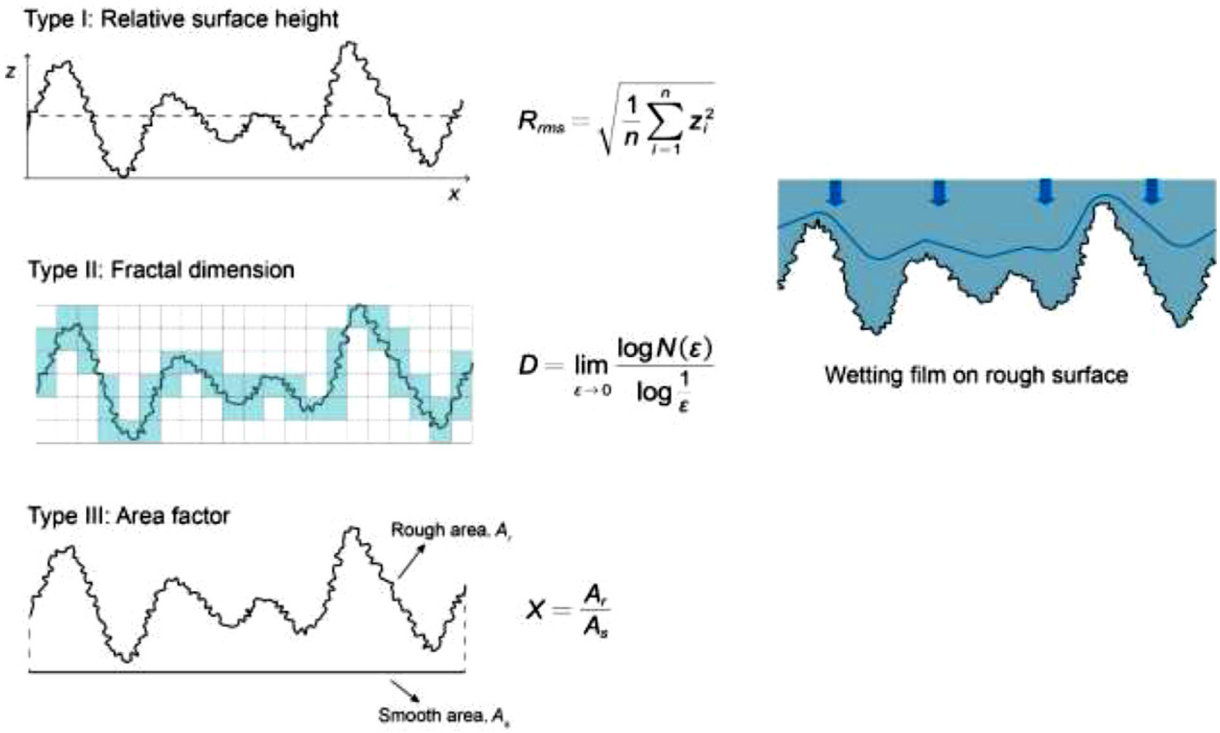

Fig. 1. Types of representations of surface roughness. (i) Relative surface height, calculated as the average elevation (usually root-mean-square, R_{rms}) to a reference coordinate axis. (ii) Fractal dimension (D), shown as the box-counting dimension, which is calculated by covering the fractal curve with box grids of equal side length (ε) and counting the number of boxes required (N). (iii) Area factor (X), calculated as the ratio of the cumulative rough area (A_r) and a reference smooth area (A_s). Configuration of a wetting film on rough surface is plotted in the right column.

noted that a related characterization is sometimes employed, the Hurst roughness exponent. This term is related to the fractal dimension, and ranges from 0 to 1 . The third definition was proposed by Wenzel (1936), in which surface roughness was defined as an area factor, e.g., the ratio of "actual surface area" over "geometric smooth-surface area". Some studies have used this definition to modify flow equations or evaluate fluid-fluid interfacial area (e.g., Philip, 1978; Liu et al., 2014; Zheng et al., 2015; Jiang et al., 2020).

Another challenge for an explicit fluid-surface function is the method of characterization of surface roughness, especially for the inner pore surfaces of natural porous media. Most reports of grain surface roughness based on relative surface height are obtained by direct measurements, such as laser profilometry and atomic force microscopy (AFM) (e.g., Tokunaga et al., 2003; Kim et al., 2012), or photogrammetric reconstruction of images obtained from scanning electron microscopy (SEM) (e.g., Kibbey, 2013). However, these methods have very small fields of view (e.g., less than 100 μm in one dimension in AFM), which brings about uncertainties at larger scales. An alternative approach is to characterize surface roughness from soil hydraulic measurements, thereby capturing larger-scale effects. For instance, fractal-dimension definitions (Ghanbarian et al., 2016; Pachepsky et al., 1995; Perfect, 1999) and area-factor definitions (Or and Tuller, 2000; Zheng et al., 2015) of surface roughness have been reported in modeling works that were extracted from measurements of soil-water characteristic (SWC) curves or unsaturated hydraulic conductivity. A limitation to this approach is that these SWC and unsaturated hydraulic conductivity data may not be highly sensitive to roughness and its influence on wetting-fluid configuration.

Measurements from gas-phase interfacial partitioning tracer tests (IPTT) have shown that total (film+meniscus) air-water interfacial areas (A_{nw}) in natural porous media increase exponentially at lower wetting-fluid saturations (S_w) (Kim et al., 1999; Costanza-Robinson and Brusseau, 2002; Peng and Brusseau, 2005; Brusseau et al., 2006). Comparison between the measurements from gas-phase IPTT, aqueous-phase IPTT, and X-ray microtomography revealed that the exponential increase is due to the significant involvement of surface roughness to film-associated interfaces at lower saturations (Brusseau et al., 2007). This is supported by the results of pore-scale modeling conducted using models that either implicitly (Or and Tuller, 1999) or explicitly (Jiang et al., 2020) account for surface roughness and its impacts on interfacial area.

The experimental and modeling results demonstrate that the A_{nw} – S_w function is highly sensitive to surface roughness, particularly at lower water saturations. Based on this behavior, Jiang et al. (2020) proposed using measured A_{nw} – S_w functions as a "wetting-film characteristic curve" to provide robust characterization of surface roughness and its interaction with wetting-fluid films. With this approach, the gas-phase IPTT method can be used to conduct measurements of total A_{nw} for a specific soil, and these data can be used to characterize fluid-surface interactions specific to that soil. It is anticipated that this approach would have multiple advantages, including greater sensitivity compared to other macroscale approaches, the ability to support both fractal-dimension and area-factor definitions, and provide characterization of surface roughness across a broader range of scales.

In the present study, we develop a general approach to characterize fluid-surface interactions and the associated model parameters from gas-phase IPTT measurements. This effort is based on the pore-scale model reported in our prior paper, which employs a triangular-pore-space bundle-of-cylindrical-capillaries (BCC) representation of the porous medium to characterize the impact of surface roughness on fluid-fluid interfacial area (Jiang et al. 2020). The basic principles of characterization are universal, which can be implemented via most of the current pore-scale models (i.e., bundle-of-cylindrical-capillaries, pore-network, pore-morphology, Lattice-Boltzmann). We use published IPTT measurements reported for four soils, and generate the characteristic parameters for each sample. We also test the validity of the characterization approach for different conditions. In addition, we have conducted

SEM imaging at different magnifications for each soil to visualize and verify the representation of surface roughness parameters. The present approach can be used to quantify fluid-solid and fluid-fluid interfacial interactions for a wide range of environmental problems.

2. Model

The present work is based on the previous study of Jiang et al. (2020). Essential concepts of the Jiang et al. (2020) model are briefly discussed herein. Variables and equations that are not specifically given in the following sections are listed in Appendix A. More comprehensive explanations of the basis and limitations of the model can be found in the original study of Jiang et al. (2020), wherein the physical, mechanistic basis for the approach is established.

2.1. General theory

Experimental and simulation evidence has indicated that wetting films on grain surfaces are held by a combination of surface adsorption (DLVO) and capillary forces (e.g., Kim et al., 2012; Tokunaga, 2011). The dominant force depends on matric potentials, and thus wetting-phase saturations, as well as the properties of the surface. Wetting films are only a few molecules thick when surface adsorption completely dominates, in which case the film surface area (and concomitantly the fluid-fluid interfacial area) is equivalent to the solid surface area obtained from gas adsorption experiments (e.g., nitrogen-BET). When capillarity dominates, film thickness increases such that the film may partially or fully cover the solid surface roughness. In the extreme case of full coverage, the wetting film can be regarded as smooth. Jiang et al. (2020) presented the concept of minimum and maximum theoretical $A_{nw} - S_w$ functions, with the actual behavior observed dependent upon a number of factors. This concept is illustrated in Fig. 2a by a theoretical "Fluid-Surface Triangle", which illustrates the function of surface adsorption and capillarity with respect to fluid-fluid interfacial area.

The fluid-surface triangle is anchored by a zero interfacial area at $S_w = 1$ and two points at $S_w = 0$: a "smooth" specific solid surface area (A_s) and a "rough" specific solid surface area (A_r), which follows the assumption that the maximum interfacial area is equal to the solid surface area (Or and Tuller, 1999; Peng and Brusseau, 2005; Jiang et al., 2020). The lower and upper curves correspond to two imaginary cases of "smooth-surface" and "maximum-roughness", respectively. For the smooth-surface curve, it is assumed that no surface roughness exists in grain surfaces, or equivalently that surface roughness is completely masked by thick wetting films at all saturations. For the maximum-roughness curve, it is hypothesized that only surface adsorption participates in the configuration of wetting film, so that the area of wetting film is always identical to the rough solid surface covered by the wetting film.

The two limits of the surface-fluid triangle are determined by the inherent properties of the specific porous medium. The smooth-surface curve is controlled simply by the pore structure and pore-size distribution of the medium. Conversely, the maximum-roughness curve indicates the greatest degree to which surface roughness can affect wetting film area. The extent can be derived from the two anchor points in the A_{nw} axis. For a rough porous medium, the surface roughness factor, X, is defined by the ratio of its rough specific surface area, A_r, to the smooth specific surface area, A_0, such that:

$$X = A_r / A_0 \tag{1}$$

Typically, A_r can be obtained from the nitrogen-BET measurement of specific solid surface area. Multiple methods are available to determine A_0, including calculation using a smooth-sphere assumption and mean particle diameter, estimation using SWC data, or measurement by X-ray microtomography.

Results of IPTT, especially the gas-phase tests at lower water saturations (< 0.4), have shown that actual A_{nw} curves reside within the fluid-surface triangle as shown in Fig. 2b. The insert in Fig. 2b illustrates the possible shape of wetting film in an actual drainage process. When capillary forces are dominant at higher saturations, the film thickness is greater than the magnitude of surface roughness, which in effect masks the impact of surface roughness. In this case, the actual A_{nw} curve will be similar to the smooth-surface curve. As wetting films become thinner and surface adsorption becomes increasingly significant at lower saturations, the contribution of surface roughness to film interfacial area increases, resulting in the exponential increase in interfacial area shown in Fig. 2b. Finally, the A_{nw} curve ascends towards the roughness-based specific solid surface area, and merges with the maximum-roughness curve. For a specific porous medium, the degree to which surface roughness is masked can vary depending on its features of fractal-scale roughness, which should be expressed via fractal dimension or area factor. Thus, it is reasonable to introduce an interfacial area factor X_a, which is always

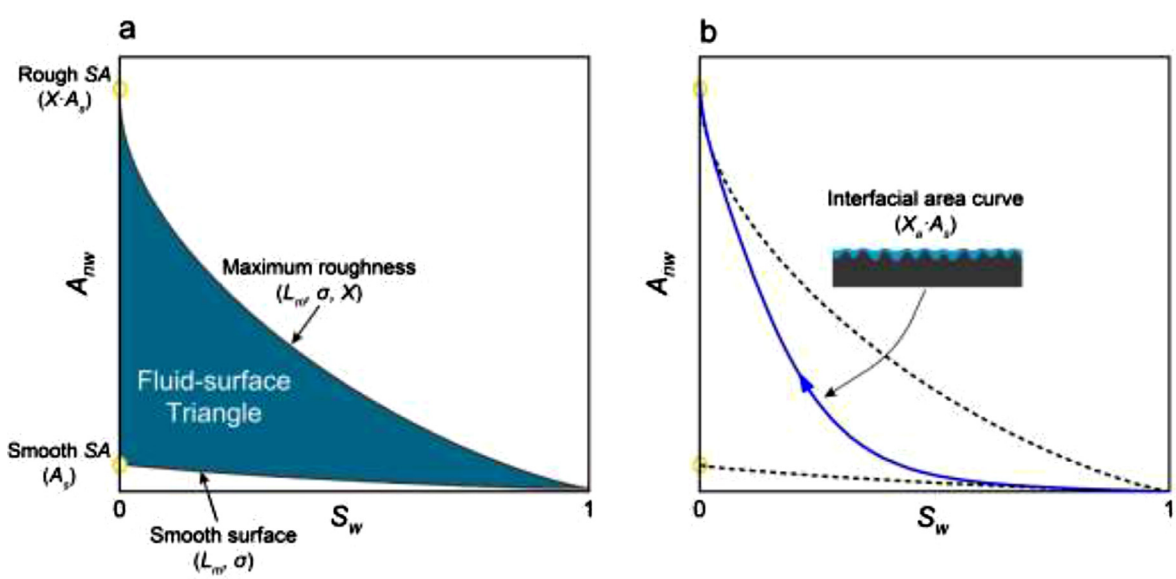

Fig. 2. Illustration of (a) the "Fluid-Surface Triangle" for the $A_{nw} - S_w$ relationship, and (b) the location of an actual $A_{nw} - S_w$ curve. Model parameters corresponding to each curve are marked. A_{nw} has units of cm^2/cm^3 or cm^{-1}.

lower than the solid surface roughness factor X, such that:

$$X_a = A_{nw}/A_0 \tag{2}$$

It is worthwhile to note that X in Eq. (1) only depends on the properties of the soil, but X_a in Eq. (2) is a function of saturation, and ultimately, matric potential. Therefore, for a universal approach to characterize surface roughness from sample-scale measurements of soils, the methodology requires two steps: (i) determination of the value of X; (ii) determination of X_a as a function of saturation or matric potential.

2.2. Characterization model

Following the approached developed in Jiang et al. (2020), the bundle of cylindrical capillaries (BCC) method is selected to establish the characterization model. The major advantage of BCC over other modeling approaches (e.g., pore-network) is the specification of pore-size distribution for a specific porous medium, which facilitates incorporation of the surface roughness representation of X and X_a in accordance with experimental data. In addition, the simplification from 3D to 2D pore geometry in the BCC model has been validated in various studies on porous media (Dahle et al., 2005; Diamantopoulos et al., 2016; Helland and Skjaeveland, 2007; Or and Tuller, 1999). The justification for using this approach is fully described in Jiang et al. (2020).

In the present BCC model, a porous medium is approximated as a bundle of equilateral triangular pores, whose side length, L, follows a lognormal distribution, $f(L)$:

$$f(l) = \frac{1}{L\sigma\sqrt{2\pi}} \exp\left(-\frac{\left[\ln\left(L/L_m\right)\right]}{2\sigma^2}\right) \tag{3}$$

The two parameters L_m and σ are the mean side length and logarithm standard deviation for lognormal distribution, respectively. For an unsaturated smooth porous medium, both specific solid surface area (A_s) and interfacial area (A_{nw}) are only controlled by the pore-size distribution parameters L_m and σ (see Fig. 2a). For a rough porous medium, first, it is assumed that every pore has a uniform surface roughness factor, X, defined by Eq. (1); then, under a specific matric potential, μ, the interfacial area factor, X_a, is specified on each pore surface in the form of wetting film (Fig. 1b). According to Jiang et al. (2020), X_a is assumed to follow a logistic function, which is given by:

$$X_a = \frac{X + e^{k(h_{ad}-h_m)}}{1 + e^{k(h_{ad}-h_m)}} \tag{4}$$

where the parameters k and h_m correspond to the change of wetting film in drainage under the impact of micro-scale fractal roughness. Eq. (4) is based on the experimental profiles between interfacial area (related to X_a) and matric potential (related to h_{ad}) (e.g., Brusseau et al., 2006; Kim et al., 1997; Porter et al., 2009).The rationale and support for using this equation is described fully in Jiang et al. (2020). Parameter k (unit of reciprocal length) controls the growth rate of film area in drainage, and h_m (unit of length) indicates the thickness of a critical sub-layer of roughness, which triggers the exponential increase in the $A_{nw} - S_w$ curve. The argument variable h_{ad} in Eq. (4) is a function of matric potential μ (see Appendix for the equation). With the constraints in Eq. (4), X_a is only controlled by one variable, μ, and is always limited in the range between 1 and X.

The characterization of surface roughness has been parameterized into five explicit parameters: L_m, σ, X, k, and h_m. Each of them can be determined from experimental data sets, e.g., SWC ($P_c - S_w$), solid surface area (nitrogen-BET), and IPTT ($A_{nw} - S_w$) measurements. SWC data are used to determine the pore-size distribution parameters L_m and σ, and subsequently, the overall roughness factor X can be calculated as the ratio of the measured nitrogen-BET specific surface area A_r and the smooth surface area obtained from L_m and σ. Upon obtaining L_m, σ, and X, the remaining parameters k and h_m can be obtained by fitting the model to the $A_{nw} - S_w$ data set. Determining the values of k and h_m for a specific porous medium is the critical step in the characterization procedure.

It is emphasized that all five parameters are not obtained from one single data set. Rather, three distinct and independent data sets are used to parameterize the model, SWC data for L_m and σ, nitrogen-BET for X, and IPTT data for the remaining two. The degrees of freedom in parameter determination are considerably constrained by the use of these three independent data sets, which limits the uncertainty in model output. Furthermore, the use of SWC data to characterize pore-size distributions of porous media is a widely used and well-established approach. The use of nitrogen-BET analysis to determine solid surface areas is the gold standard for characterization of surface areas. The use of IPTT data to characterize interfacial areas has been established in multiple works. Hence, use of each of the three data sets for parameter determination is well established; the combination and integration of the three into a unified approach to characterize fluid-solid interactions is the unique aspect of the present study.

The detailed procedure of optimization requires a classification of the wetting-fluid distribution in pores, which can range from fully-filled to partially-drained to fully-drained pores. In partially-drained pores, wetting fluid is distributed along the pore side walls, and form different configurations as film fluids or meniscus fluids, corresponding to film and meniscus interfacial area. Under a given drainage potential, there is a critical size of pore where the nonwetting phase begins to invade into a filled pore (onset of drainage). This critical pore size, L_1, corresponds to a geometrical constraint given by Tuller et al. (1999):

$$L_1 = \frac{\gamma}{\rho\mu} C_3 \tag{5}$$

where γ and ρ are the surface tension and density of the wetting fluid, respectively, and C_3 is a constant regarding to triangular pore geometry (see Appendix). Pores larger than that size are all partially or fully drained, with the same meniscus radius, r, controlled by the Young-Laplace law (the wetting phase is assumed to be completely wetting to the solid surface):

$$r = \frac{\gamma}{\rho\mu} \tag{6}$$

Knowing the relationship between matric potentials and critical pore sizes, the equations for capillary pressure (matric potential), saturation, and interfacial area can all be derived from pore geometry. The geometric relationships between liquid films and menisci within a triangular pore (partially-filled) are presented in Fig. 3.

Typical equations for both S_w and A_{nw} in the literature are given with matric potentials as the argument variable. To conduct the surface roughness characterization, it is assumed that the three variables coalesce into an integrated $P_c - S_w - A_{nw}$ relationship (Hassanizadeh and Gray, 1993), so as to make it convenient to implement the model optimization on $A_{nw} - S_w$ data sets. The equations for S_w and A_{nw} with the terms of all types of fluid configuration (filled-pore fluid, film fluid, and capillary-meniscus fluid) are given as (Jiang et al., 2020):

$$S_w = S_{wd}(\mu) + S_{wf}(\mu) + S_{wc}(\mu) \tag{7}$$

$$S_{wd}(\mu) = \int_{L_{\min}}^{L_1(\mu)} f(L)dL \tag{8}$$

$$S_{wf}(\mu) = \int_{L_1(\mu)}^{L_{\max}} \frac{3h(\mu)\left[L - 2r(\mu)\cot(\pi/6)\right]}{A_3 L^2} f(L)dL \tag{9}$$

$$S_{wd}(\mu) = \int_{L_1(\mu)}^{L_{\max}} \frac{3F_3 r^2(\mu)}{A_3 L^2} f(L)dL \tag{10}$$

$$A_{nw} = A_{nwf}(\mu) + A_{nwc}(\mu) \tag{11}$$

$$A_{nwf}(\mu) = \int_{L_1(\mu)}^{L_{\max}} \frac{3X_a\left[L - 2r(\mu)\cot(\pi/6)\right]}{A_3 L^2} f(L)dL \tag{12}$$

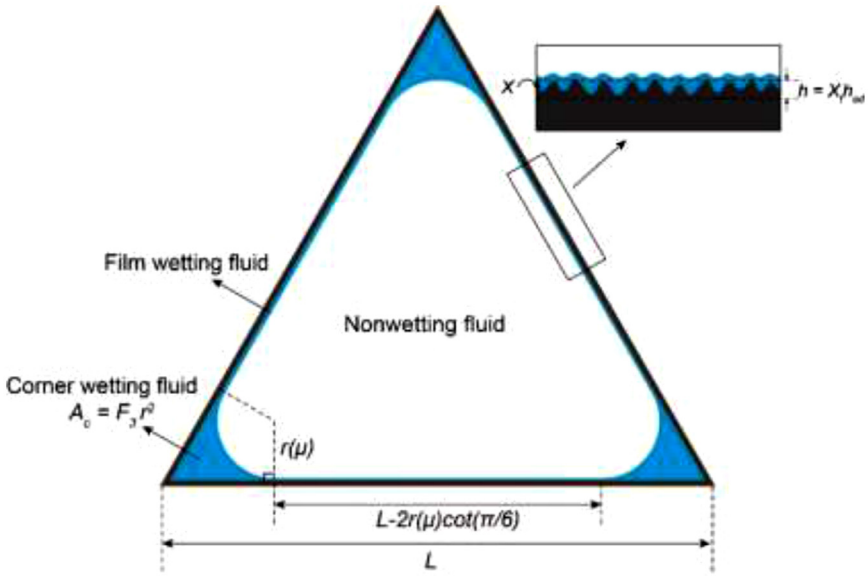

Fig. 3. Cross-sectional scheme of a typical partially-filled triangular pore (Jiang et al., 2020).

Table 1
Physical properties of the selected porous media.

Medium	Texture	Mean diameter d_m (mm)	Porosity n	Bulk density (g/cm^3)	Specific solid surface area (cm^{-1})[a]
Kim et al.	Sand	0.250	0.36	1.72	2000
Accusand	Sand	0.350	0.42	1.65	2800
Granusil	Sand	0.172	0.43	1.54	6622
Vinton	Sandy soil	0.234	0.46	1.46	51,684
Hayhook	Soil	0.260	0.36	1.64	88,000

[a] Measured with the nitrogen BET method.

$$A_{nwc}(\mu) = \int_{L_1(\mu)}^{L_{\max}} \frac{3\pi r(\mu)}{2A_3L^2} f(L)dL \tag{13}$$

The development of these equations are discussed in detail in Jiang et al. (2020).

Equations (7~10) and equations (11~13) indicate that total saturation is the sum of filled-pore (duct) fluid (S_{wd}), film fluid (S_{wf}), and capillary-meniscus fluid (S_{wc}), while total interfacial area is only determined by film (A_{nwf}) and capillary-meniscus (A_{nwc}) fluid in partially-filled pores. Definitions of $h(\mu)$, A_3, F_3, L_{min}, and L_{max} are given in the Appendix. The magnitudes of these components have been investigated in previous modeling studies (Or and Tuller, 1999; Zheng et al., 2015; Jiang et al., 2020), amongst which filled-pore fluid is dominant in saturation, and film fluid is dominant in interfacial area. It is then logical to minimize focus on the uncertainties in the less significant components during the characterization process, e.g., film fluid in fitting $P_c - S_w$ curves, and meniscus interface in fitting $A_{nw} - S_w$ curves. It is also noted that the maximum A_{nw} in Eq. (11) as $\mu \to \infty$ is equal to the rough specific surface area A_r, which represents the assumption of Fig. 2b.

3. Materials

Peng & Brusseau (2005, 2012) measured the air-water interfacial areas for various types of porous media via gas-phase IPTT. In addition, they reported the data of specific solid surface areas and soil-water characteristic curves for four media: Accusand, Granusil, Vinton, and Hayhook. Among the four porous media, Accusand and Granusil are well-sorted natural sands; Vinton is a sandy soil; Hayhook is a coarse loamy soil. The four selected porous media comprise a range of physical and geochemical properties, which are useful for the test of surface characterization methods on varying natural media. Basic soil texture properties for the studied porous media are summarized in Table 1.

Gas-phase IPTTs are limited to lower water saturations. Available A_{nw} data for higher water saturations obtained via aqueous-phase IPTT (Brusseau et al., 2007, 2015) are combined with the gas-phase IPTT data. These data are available for Accusand and Vinton. To test the generalness of the approach, aqueous IPTT data for a PCE-water system with Accusand from Zhong et al. (2016) are also chosen. Another sandy medium with interfacial area measurements by Kim et al. (1997, 1999) is also listed in Table 1 for comparisons in the following sections.

4. Results and discussion

4.1. Parameterization of surface roughness effect

Experimental evidence has shown that wetting films on natural grain surfaces are sensitive to scale. Surface adsorption can only support thin films at the magnitude of 1~10 nm (Resurreccion et al., 2011; Tokunaga, 2011), while capillary forces tend to be enhanced on rougher surfaces, resulting in thicker films at the magnitude of 0.1~1 μm (Kim et al., 2012; Tokunaga, 2011; Tokunaga et al., 2003). Among the three types of surface roughness representations in Fig. 1, the relative surface height (Type I) is limited by its primary scale for the selected range of coordinates. The fractal dimension (Type II) has been used in the simulation of soil hydraulic properties such as hydraulic conductivity and relative permeability (Ghanbarian et al., 2016; Thompson and Brown, 1991). Fractal dimension is appropriate for multi-dimensional problems with a constant D value (e.g., the perimeter and cross-section area are related by fractal dimension in tube flow), but is inconvenient for situations where D is changing, which occurs in the change of wetting film controlled by matric potentials. Conversely, the area factor (Type III) approach used in this study, especially the use of interfacial

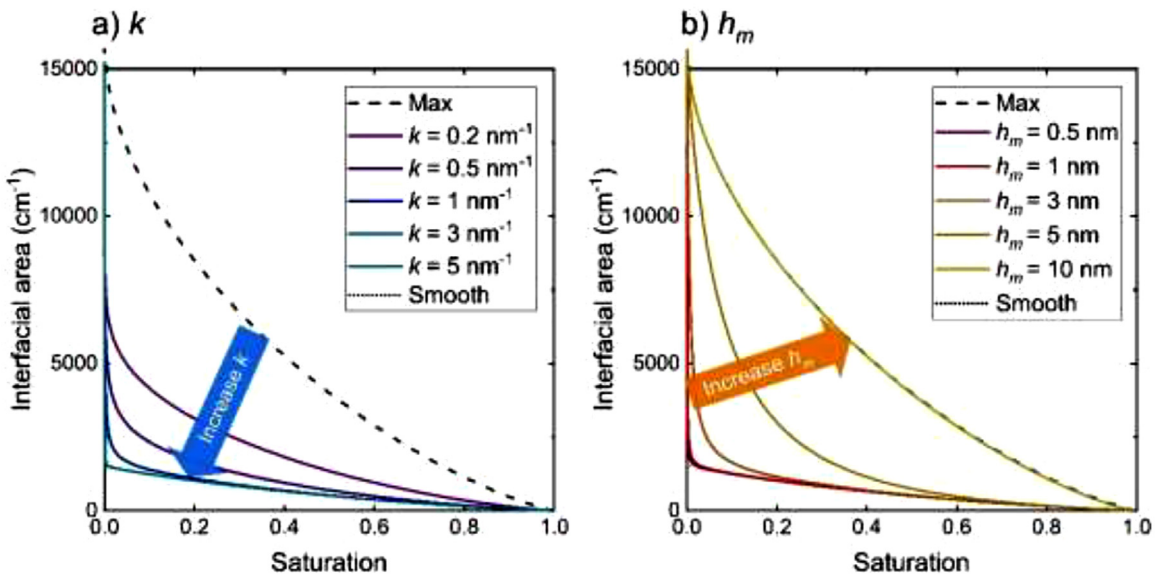

Fig. 4. Effects of changing parameter (a) k (b) h_m in the space of the surface-fluid triangle. The default values of parameters are $X = 50$, $L_m = 90$ μm, $\sigma = 0.5$, $\mu_d = -1$ J/kg, $k = 1$ nm^{-1}, and $h_m = 2$ nm.

area factor X_a, provides a convenient cross-scale methodology to parameterize the scale-sensitive interaction between fluids and solid surfaces. At the lowest matric potentials, the wetting-film interfaces will tend to be smooth, which is the lowest D. As surface adsorption dominates at higher matric potentials, the films become sufficiently thin such that their surface topology mimics the finest structures of the solid surface, representing the highest fractal dimension, which is also the D of rough solid surfaces. Therefore, the interfacial area factor X_a contains information of the fractal-scale properties of wetting films. In addition, the measurement scale for the area factor is controlled by experiment-based variables, such as nitrogen-BET measured solid A_r, matric potentials, wetting-fluid saturations, and interfacial areas, which improves the accuracy of fractal representation.

Thus, it is elucidated that the "fluid-surface triangle" defined in Fig. 2 delineates the free fractal space of wetting film interfacial area, wherein the upper (maximum-roughness) and lower (smooth-surface) curves represent the maximum and minimum fractal dimensions of the film interface, respectively. Meanwhile, the two limiting conditions determine the range for X_a, within $X_a = 1$ (smooth) and $X_a = X$ (roughness factor of solid phase). With the interfacial area factor $X_a(\mu)$ determined from IPTT experiments, the surface-fluid interaction in fractal space can be quantified and parameterized.

The logistic Eq. (4) provides a simple approach for quantifying the roughness characteristic, with only two parameters: k and h_m. The effects of k and h_m are illustrated in Fig. 4. In general, both parameters define the degree to which capillary forces mask the solid surface roughness beneath a wetting film, as is shown by the phenomenon that some portions of the $A_{nw} - S_w$ curves are coincident with the smooth-surface curves in both plots. Inspection of Fig. 4 indicates that either increasing k or decreasing h_m can enhance the degree of masking. In addition, the trends of changes are different for k and h_m: in an $A_{nw} - S_w$ plot, k controls more of the horizontal region of A_{nw} curves (the higher saturation region), while h_m has a stronger influence on the vertical region (lower saturations).

Based on the mathematical features of the logistic function and fractal geometry, we are able to develop the physical representations for parameters k and h_m. First, as a variable with the dimension of length, h_m corresponds to a critical matric potential, which is normalized as "critical adsorptive thickness" in the logistic function, such that wetting film thickness approaches the magnitude of the critical manifestation of fractal roughness. It is noted that the actual wetting film thickness at this stage is not equal to h_m, as the involvement of capillary forces in wetting film is still significant. The equation to calculate this film thickness is given in the Appendix. Larger values of h_m cause the exponential stage of $A_{nw} - S_w$ curves to start earlier, i.e. at higher saturations.

The exponential parameter k determines the growth rate of the logistic curve, which is, from another perspective, a representation of the complexity of the fractal structure of the surface. This term can be conceptualized as "thickness per area". Surfaces with smaller k values have smaller degrees of surface-roughness masking for the $A_{nw} - S_w$ curves. Thus, the curves exhibit a more uniform rate of increase as saturation decreases. This indicates that surfaces with smaller k values comprise a greater number of fractal iterations between smooth surface and maximum roughness, or between the varying ranges of fractal dimensions. It is important to note that the influence of surface charge, wettability, and other factors on the formation and disposition of wetting films is implicitly incorporated in the model through these two parameters (Jiang et al., 2020).

4.2. Characterization results

Results of the fitted curves generated by the characterization model are illustrated in Fig. 5 in comparison with the measured data of $P_c - S_w$ and total $A_{nw} - S_w$. All simulated curves are generated by the optimization toolbox in MATLAB. It is shown that the model produces very good fits of the measured data. The lognormal pore size distribution parameters L_m and σ are derived from the $P_c - S_w$ data sets, the solid roughness factor X is determined from the solid specific surface area measured via nitrogen-BET, and the logistic parameters k and h_m are derived from the total $A_{nw} - S_w$ data sets. Overall, the good matches of the measured data for all four media shows that the proposed parameters and mathematical assumptions are sufficient to address the characteristics of surface roughness for natural granular media. One possible source of uncertainty is the values of lognormal standard deviation, which is affected by some inconsistencies on the low saturation data of $P_c - S_w$ curves. However, as discussed by Jiang et al. (2020), the standard deviation has very little impact on the determination of interfacial area parameters.

Values of the fitted model parameters, along with some other parameters of soil texture, e.g., median particle diameter d_{50} and uniformity coefficient U calculated by d_{60}/d_{10} are given in Table 2 accord-

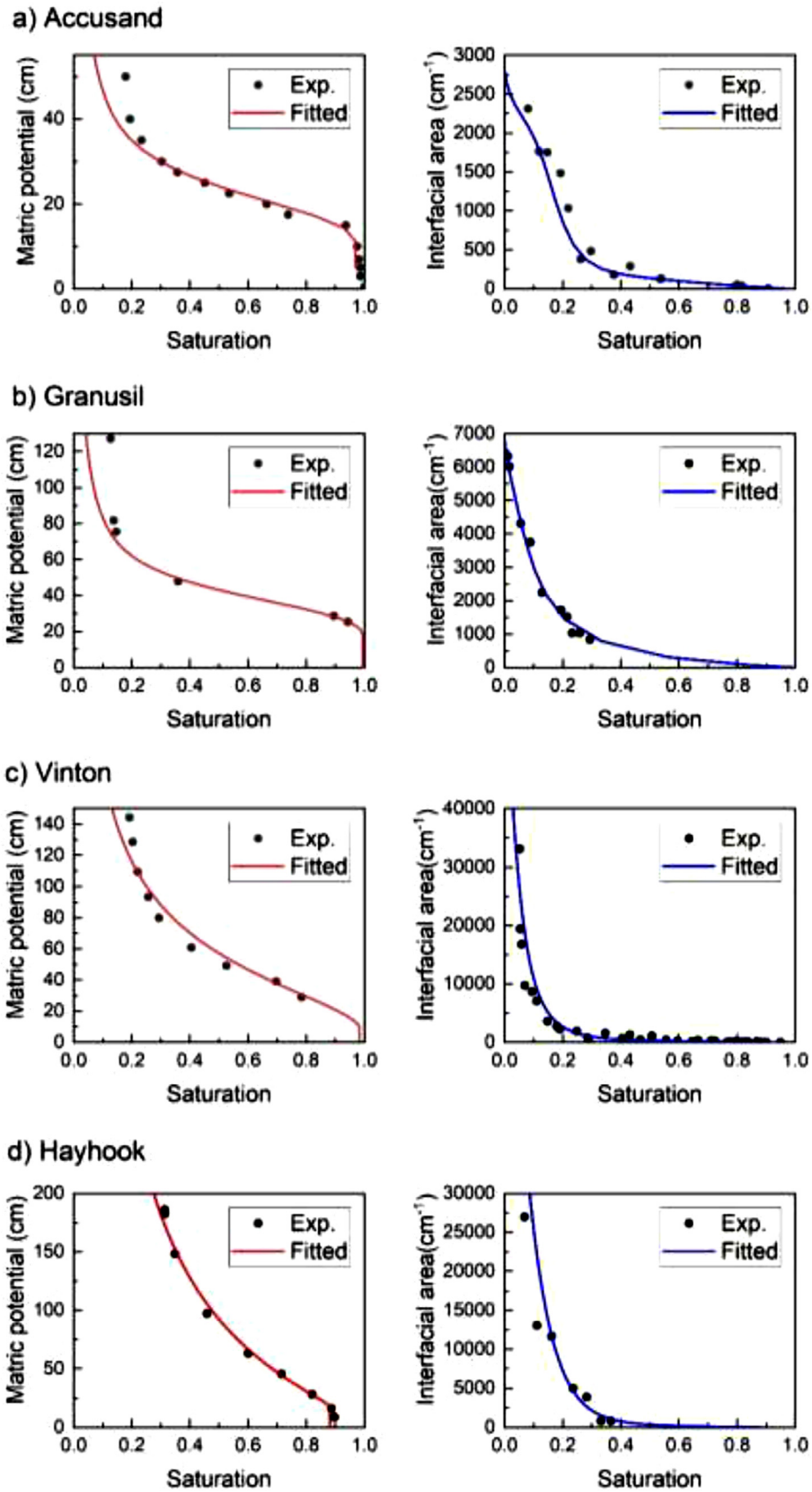

Fig. 5. Model characterization results for the experimental data of $P_c - S_w$ and $A_{nw} - S_w$ measurements. The measured data are from Peng and Brusseau (2005).

Table 2
Parameters of soil texture, pore size distribution, and surface roughness properties for the selected porous media.

	Soil texture		Solid surface roughness		Pore size distribution		Micro-scale fluid-solid		
Parameter	d_{50} (μm)	$U = d_{60}/d_{10}$	A_r(cm^{-1})	X	L_m (μm)	σ	K (nm^{-1})	h_m (nm)	h_c (nm)
Kim et al.	250	N/A	2000	5.0	171.0	0.164	2.1	6.3	4.0
Accusand	350	1.16	2800	8.7	212.7	0.303	3	9.7	8.5
Granusil	172	1.77	6622	11.3	116.4	0.251	1.5	7.5	9.2
Vinton	234	2.4	51,684	58	93.6	0.685	1.8	5.2	26.3
Hayhook	260	16	88,000	40.6	58.0	1.119	0.75	3.3	11.9

Soil texture data from Peng and Brusseau (2005).

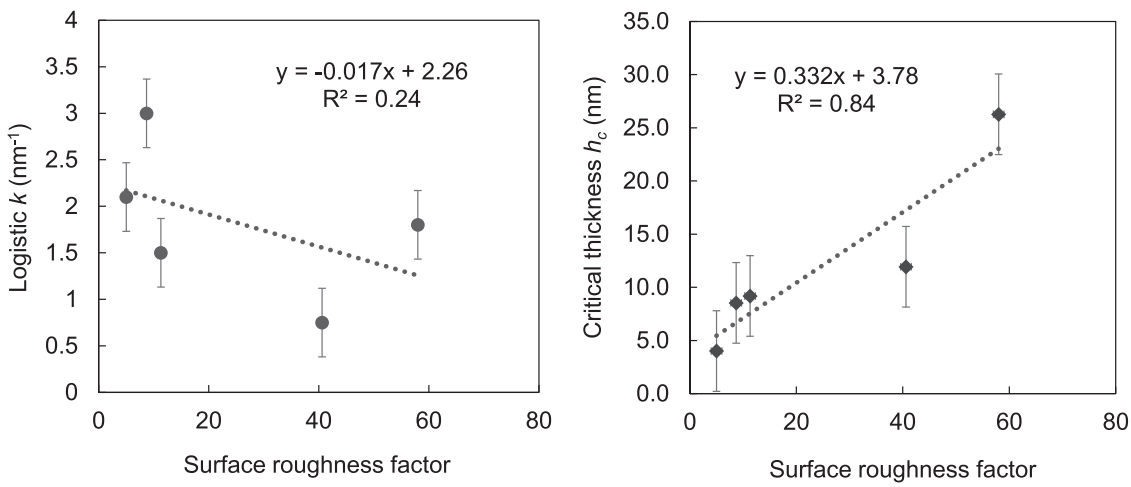

Fig. 6. Correlations between micro-scale surface roughness characteristics and the solid surface roughness factor X.

ing to the reported data (Peng and Brusseau, 2012). The results from another model test run on the literature data reported by Kim et al. (1997, 1999) are also listed in Table 2. The actual critical film thickness, h_c, which corresponds to the value of h_m, is calculated via the empirical film thickness equation given in Zheng et al. (2015) (see Appendix), showing the combined contributions of surface adsorption and capillarity to film thickness. In the view of surface roughness characterization, the primary concern is whether there are quantitative correlations between the surface roughness-related parameters and the sample-scale features, such as particle and pore-size distribution.

Characterization results in Table 2 show that the traditional sample-scale parameters, e.g., uniformity coefficient U, lognormal average pore size length L_m, specific surface area A_r, and the solid roughness factor X, all show some degree of correlations with soil texture, especially between sands and soils. The one exception for the solid surface roughness factor is that of Hayhook, which is smaller than that of Vinton even though the former has a 70% larger specific solid surface area and a larger uniformity coefficient.

To test potential correlations between micro-scale roughness properties and the sample-scale soil properties, results between k vs X and h_c vs X are plotted in Fig. 6. The logistic parameter k is poorly correlated to surface roughness factor X for the five media used in this study. Thus, it would be difficult to predict the fractal surface properties of natural porous media from soil texture. For instance, Vinton has far more specific surface area than Granusil, but it also has a larger value of k as well as a smaller h_m. Consequently, the $A_{nw} - S_w$ curve of Vinton, in terms of Fig. 4a, could be closer to the smooth-surface curve at some saturations, meaning that Vinton has stronger surface roughness masking than Granusil. As noted above, k represents the complexity of the fractal structure of the surface, whereas X represents the overall magnitude of surface roughness (roughness capacity). The fractal complexity of natural solid surfaces is expected to vary greatly among different media, as is illustrated in the following section. Thus, it is reasonable to anticipate that different media that have similar overall magnitudes of surface roughness (i.e., similar X values), may have different fractal structuring (different k values). Such behavior would explain the poor correlation between the two variables. A larger data base would be needed to further test this relationship.

Conversely, the critical thickness h_c presents some degree of correlation with X ($R^2 = 0.84$), which implies that rougher grain surfaces can induce the exponential increase of interfacial area at larger measurement scales (larger saturations).

The quantitative results in Table 2 and Fig. 6 demonstrate the complexity of fluid-surface interactions. The interplay between surface adsorption and capillary forces for wetting film is assumed to occur at scales much smaller than the size of soil particles, and even smaller than the magnitude of relative surface height. Fluid-surface interaction on such micro-scale rough structures is controlled by the complicated and chaotic nature of fractal growth. Furthermore, the meso-scale (between single particle and finer structures) surface heterogeneity, such as pits and fractures on single grain surfaces (Araújo and Brusseau, 2019), would also increase the complexity of fractal properties for micro-scale roughness. This illustrates the importance of surface roughness characterization for improved characterization of wetting film and its subsequent hydraulic properties.

4.3. Analysis of SEM images

The present modeling approach provides a different perspective to view surface roughness based on measured data for fluid-fluid interfacial areas. Introduction of inherent solid phase roughness parame-

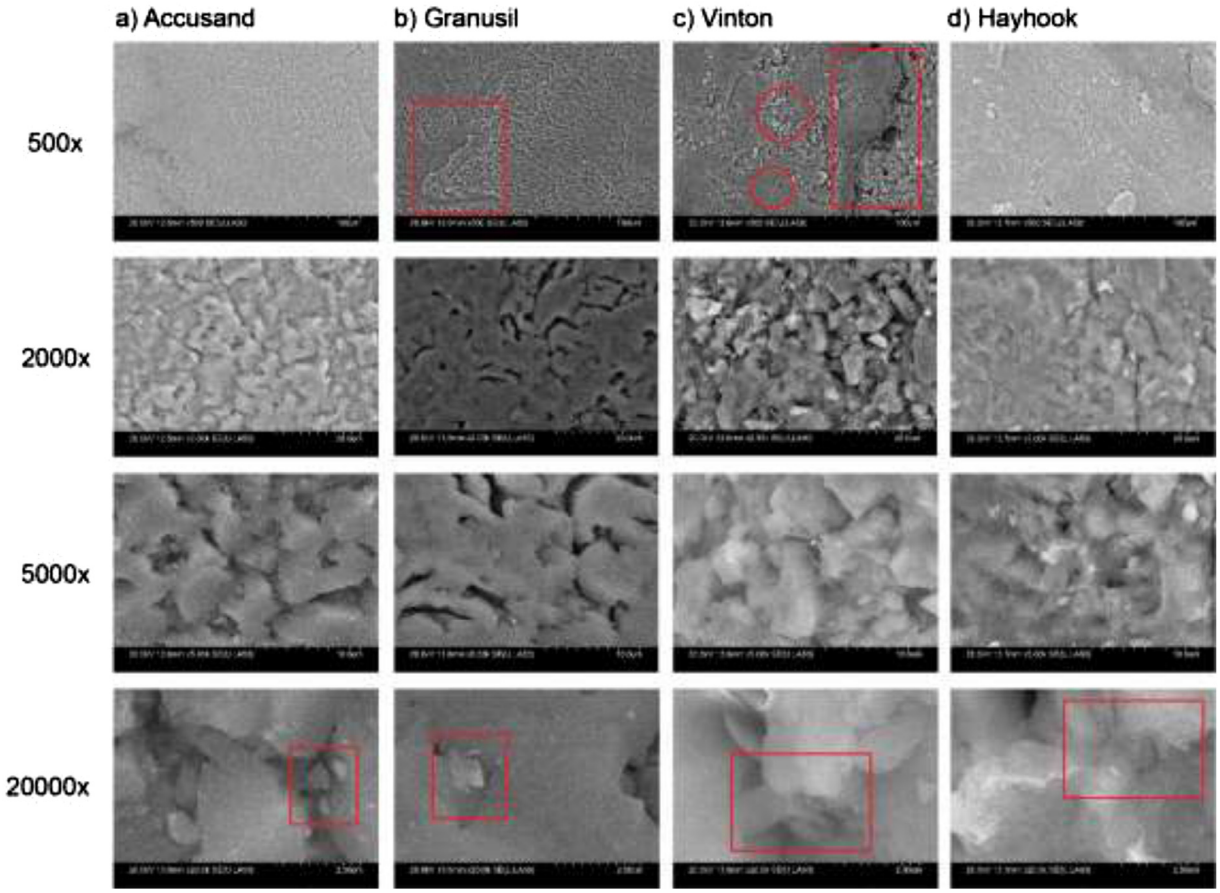

Fig. 7. SEM images of the grain surfaces of the selected porous media. The red boxes in the 500x images show examples of meso-scale structures on the surfaces of Granusil and Vinton. Circles in the 500x images of Vinton show the distinctive apparent meso-scale roughness of Vinton. Boxes in the 20000x images indicate the typical structures that are critical for further growth of surface area.

ters can avoid the scaling bias of direct measurement such as SEM or AFM, whereby higher resolutions lead to smaller measurable regions. To demonstrate these phenomena and compare with the characterization results, SEM images of the four porous media (Accusand, Granusil, Vinton, and Hayhook) used in this study are obtained with a series of magnifications (500x, 2000x, 5000x, 20000x) (see Fig. 7). The minimum and maximum magnifications (500x and 20000x) represent a change in image domain from approximately 35,000 μm^2 to 40 μm^2 and resolutions from micrometer to nanometer scales. Images were obtained with a Hitachi S-4800 Field Emission SEM in the Kuiper Materials Imaging & Characterization Facility of the University of Arizona. SEM images are used to analyze visual associations between the real images of natural grain surfaces and the surface roughness parameters X, k, and h_m (h_c).

First, some meso-scale features, such as fractures on grain surfaces, can be identified from the 500x SEM images, as highlighted with the red boxes for Granusil and Vinton. The sub-iterations of these heterogeneous structures are obviously different from the more homogeneous surface domains. It is also observed that the meso-scale surfaces of Vinton appear more divergent than other media, as is indicated by the circles of two surface regions with highly distinctive apparent roughness. This may partially explain the apparently anomalous value of k for Vinton. To mitigate the uncertainties from heterogeneity, the following magnified regions are selected to the seemingly roughest sites in the 500x images. The 2000x and 5000x images correspond to the reported magnitudes (0.1~1 μm) of relative surface height representation (Adams et al., 2012; Kim et al., 2012; Tokunaga et al., 2003). All media show apparent uniform surface structures at these two levels. It could be assumed that wetting films at these scales are held primarily by capillary forces and remain sufficiently thick. However, the potential for additional roughness scales for the soil media (Vinton and Hayhook) is manifest in the 5000x images, while the sandy media (Accusand and Granusil) exhibit a larger proportion of smoothness in the images.

In the 20000x images, the thickness of roughness layers is in the range of tens of nanometers, close to the magnitudes of critical thickness (h_c) in Table 2. It is possible to recognize the iterated sub-layers of fractal roughness at this level. Inspection of the 20000x images provides a possible verification to the correlation between critical thickness and surface roughness factor exhibited in Fig. 6. At this level, the sandy media (Accusand and Granusil) only have a limited number of small and flat structures (as indicated in images) contributing to surface area, while the soil media (Vinton and Hayhook) present larger and deeper roughness formations that allow for further iterations of roughness scales. Such differences explain the differences in the nitrogen-BET surface areas between the sands and soils. However, it is also noticeable that surface information at this magnification has been considerably lost. It would be difficult to establish the explicit quantitative connections between the characterization results and the SEM images at this degree of magnification. Rather, it is further highlighted that the characterization approach based on sample-scale measurement has the unique capability of extracting the micro-scale information of fluid-solid interaction that is operationally relevant to flow and transport, which is difficult to ascertain from imaging methods.

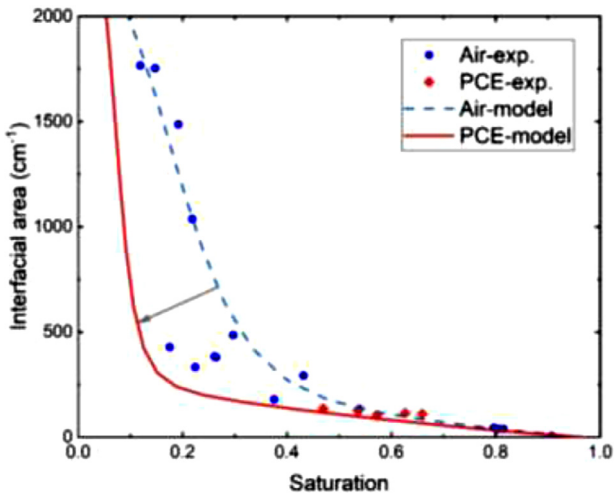

Fig. 8. Test for air-water and PCE-water interfacial areas measured from IPTT. Air-water curve (blue dashed line) is fitted to the measured data points. PCE-water curve (solid red line) is predicted using the model parameters obtained from calibration to the air-water data. Saturation in the x-axis corresponds to the wetting fluid (water).

4.4. Application to NAPL-water fluid systems

The generalness of the surface roughness characterization method is based upon the premise that solid surface roughness remains constant regardless of any arbitrary flow conditions. Actual environmental problems can involve fluids with different properties, such as immiscible (nonaqueous phase) organic liquids (NAPL). Hence, a limited test is conducted in this section using published experimental data for the same Accusand but with a different nonwetting fluid (NAPL). The results are presented in Fig. 8. Air-water A_{nw} measurements are reported in Brusseau et al. (2015) and Peng & Brusseau (2005), and NAPL-water A_{nw} measurements using tetrachloroethene (PCE) are reported in Zhong et al. (2016). To implement the test, the parameters L_m, σ, X, k, and h_m determined for the air-water Accusand data are directly applied to the PCE-water data. The only adjustment is by substituting the surface tension γ for water with the interfacial tension between PCE and water. Values used in Fig. 8 are 0.0728 N/m for air-water and 0.0459 N/m for PCE-water.

As is shown in Fig. 8, the predicted PCE-water A_{nw} curve matches the measured data points. This suggests that there is generalness in the approach for characterizing wetting-film configuration. Greater roughness masking is observed for the NAPL-water system compared to the air-water system at lower wetting-fluid saturations. However, at higher saturations, interfacial areas for both fluid pairs are similar. Similar experimental evidence was reported by Schaefer et al. (2000a, 2000b), in which air-water and NAPL-water fluid-pairs exhibited similar interfacial areas for mass-distribution–based IPTT measurements over a large range of saturation. However, such measurements do not fully access the adsorption-dominant wetting film at very low saturations, whose properties are better captured by the gas-phase IPTT measurements.

A recent comparison of IPTT data for NAPL-water systems demonstrated that similar NAPL-water interfacial areas were measured for different fluid pairs for the same porous medium (Brusseau and Taghap, 2020). The data sets included PCE-water, decane-water, and hexadecane-water pairs. This provides some indication that fluid properties that affect multi-phase flow in porous media, such as density, viscosity, and spreading coefficient, may not have significant impact on the inherent interfacial area of the system. Thus, it is anticipated that the IPTT characterization method will provide robust determination of interfacial areas for application to different fluid pairs.

5. Conclusions

A methodology is developed to employ measured $A_{nw} - S_w$ curves to characterize the fluid-surface interaction controlled by micro-scale surface roughness of porous media solids. The method is based on a general theory of adsorbed wetting films on rough solid surfaces, where the films are held by some combination of surface adsorption and capillary forces. The characterization is realized by quantifying the change of film-associated fluid—fluid interfacial area between capillary-dominant states (smooth film) and adsorption-dominant states (rough film) controlled by matric potentials. As the quantification of wetting-film formations employs use of sample-scale measurements of porous media (e.g., nitrogen-BET and IPTT), it provides an effective approach to conceptualize and simulate the multiple scales of roughness associated with the fractal geometry of natural grain surfaces. The wetting-film vs matric-potential approach incorporates the advantages of surface roughness representations using both fractal dimension and area factor, which expands the scope of grain surface roughness beyond the traditional approach of relative surface height. The use of IPTT measurements establishes a complete characterization of fluid-surface interaction across all grain surfaces within a porous medium, which is free of the spatial measurement-scale limitations influencing traditional surface metrological approaches such as SEM and AFM.

The model characterization and SEM imaging results for the selected porous media in this study highlight the complexity of natural grain surfaces. The surface heterogeneity of natural grain surfaces is present across multiple scales – from sample and particle scales, to the meso-scale on one grain surface, and then to the micro-scale surface roughness following fractal dimensions. Given the complicated nature of grain surfaces, the well-developed experimental measurement of fluid-fluid interfacial area, especially the low-S_w measurement using gas-phase interfacial tracers, provides a reliable and controllable approach to characterize the surface properties based on the formation of wetting film. The proposed characterization methodology is applicable to a wide range of environmental systems involving flow, transport, and mass transfer.

Declaration of Competing Interest

The authors declare that they have no known competing financial interests or personal relationships that could have appeared to influence the work reported in this paper.

CRediT authorship contribution statement

Hao Jiang: Conceptualization, Methodology, Investigation, Formal analysis, Data curation, Writing - original draft. **Bo Guo:** Data curation, Methodology, Supervision, Writing - review & editing. **Mark L. Brusseau:** Conceptualization, Methodology, Data curation, Writing - review & editing, Supervision.

Acknowledgements

This research was supported in part by a grant from the NIEHS Superfund Research Program (P42 ES04940). We acknowledge NASA grants #NNX12AL47G, #NNX15AJ22G and #NNX07AI520, and NSF grants #1531243 and #EAR-0841669 for funding of the instrumentation Hitachi S-4800 Field Emission SEM in the Kuiper Materials Imaging and Characterization Facility at the University of Arizona. We thank the reviewers for their constructive comments.

Appendix. Summary of Model Parameters and Derivations

Parameter	Nomenclature	Dimension	Annotation	Equation
Fluid properties				
ρ	Density of wetting fluid	ML^{-3}		
γ	Surface or interfacial tension	$ML^{-1}T^{-2}$	Can be switched to different fluid pairs.	
Variables capable of direct measurement				
μ	Matric potential	L^2T^{-2}	Equivalent to capillary pressure P_c or pressure head H.	$\mu = gH$ $P_c = \rho\mu$
S_w	Wetting-fluid saturation	—		
A_{nw}	Nonwetting-wetting interfacial area	L^{-1}	Referred to the total interfacial area, but almost equal to film-associated area at most S_w. Measured by IPTT.	
A_r	Specific solid surface area (rough surface area)	L^{-1}	Measured by N_2/BET.	
Parameters in wetting film model				
X	Overall surface roughness factor	—	Ratio of rough surface area over smooth surface area for the porous medium	$X = A_r/A_s$
X_a	Interfacial area factor	—	Ratio of film area over smooth surface area. Function of matric potential.	$X_a = A_{nv}/A_s$
$h_{ad}(\mu)$	Adsorptive film thickness	L	Film thickness with only surface adsorption. Function of matric potential.	$h_{ad}(\mu) = \sqrt[3]{\frac{A_{svl}}{6\pi\rho\mu}}$
$h(\mu)$	Actual film thickness	L	Film thickness with both capillary and surface adsorption.	$h(\mu) = X_t h_{ad}(\mu)$
X_t	Film thickness factor	—	Calculated by empirical equation (Zheng et al., 2015).	$X_t = \begin{cases} X & h_{ad} \geq 10\text{nm} \\ X(\frac{h_{ad}(\mu)}{10})^{\ln X/(\ln 200 - \ln 7)} & 0.35\text{nm} < h_{ad} < 10\text{nm} \\ 1 & h_{ad} \leq 0.35\text{nm} \end{cases}$
A_{svl}	Hamaker constant	ML^2T^{-2}	Given in literature (Or and Tuller, 1999; Tokunaga, 2011)	$A_{svl} = 6 \times 10^{-20}$ J
k	Logistic growth rate factor	L^{-1}	Given by logistic function of X_a.	$X_a = \frac{X + e^{k(h_{ad} - h_m)}}{1 + e^{k(h_{ad} - h_m)}}$
h_m	Critical adsorptive film thickness	L		
Parameters in sample upscaling				
$r(\mu)$	Meniscus radius	L	Given by Young-Laplace equation.	$r(\mu) = -\frac{\gamma}{\rho\mu}$
L	Pore side length	L	Side length of an equilateral triangular pore.	
L_m	Mean pore side length	L	Given by lognormal equation.	$f(l) = \frac{1}{L\sigma\sqrt{2\pi}} \exp(-\frac{[\ln(L/L_m)]}{2\sigma^2})$
σ	Lognormal standard deviation	—		
$L_1(\mu)$	Critical pore size	L	Pore side length at the onset of drainage.	$L_1 = \frac{\gamma}{\rho\mu} C3$
L_{min}	Minimum pore side length	L	Set as a very small number.	$L_{min} = 5 \times 10^{-9}$ m
L_{max}	Maximum pore side length	L	Pore size associated with air-entry potential.	$L_{\max} = L_1(\mu) + 2h(\mu_d)$
μ_d	Air-entry potential	L^2T^{-2}	Can be derived from Brooks & Corey method.	
F_3	Corner area factor	—	Geometric factor for equilateral triangles.	$F_n = 3\sqrt{3} - \pi$
A_3	Pore area factor	—	Geometric factor for equilateral triangles.	$A_3 = \sqrt{3}/4$
C_3	Drainage blob radius factor	—	Geometric factor for equilateral under drainage.	$C_3 = 2[\sqrt{3} + \sqrt{\pi/\sqrt{3}}]$

References

Adams, T., Grant, C., Watson, H., 2012. A simple algorithm to relate measured surface roughness to equivalent sand-grain roughness. Journal ISSN 2929, 2724.

Araújo, J.B., Brusseau, M.L., 2019. Novel fluid-fluid interface domains in geologic media. Environ. Sci.: Processes Impacts 21 (1), 145–154. https://doi.org/10.1039/c8em00343b.

Brown, S.R., 1987. Fluid flow through rock joints: the effect of surface roughness. J. Geophys. Res.: Solid Earth 92 (B2), 1337–1347.

Brown, S.R., 1989. Transport of fluid and electric current through a single fracture. Geophys. Res. Lett. 94 (2), 9429–9438.

Brusseau, M.L., Taghap, H., 2020. NAPL-water interfacial area as a function of fluid saturation measured with the interfacial partitioning tracer test method. Chemosphere 260, 127562.

Brusseau, M.L., Peng, S., Schnaar, G., Costanza-Robinson, M.S., 2006. Relationships among air-water interfacial area, capillary pressure, and water saturation for a sandy porous medium. Water Resour. Res. 42 (3).

Brusseau, M.L., Peng, S., Schnaar, G., Murao, A., 2007. Measuring air– water interfacial areas with x-ray microtomography and interfacial partitioning tracer tests. Environ. Sci. Technol. 41 (6), 1956–1961.

Brusseau, M.L., El Ouni, A., Araujo, J.B., Zhong, H., 2015. Novel methods for measuring air–water interfacial area in unsaturated porous media. Chemosphere 127, 208–213.

Cassie, A.B.D., Baxter, S., 1944. Wettability of porous surfaces. Trans. Faraday Soc. 40, 546–551.

Costanza-Robinson, M.S., Brusseau, M.L., 2002. Air-water interfacial areas in unsaturated soils: evaluation of interfacial domains. Water Resour. Res. 38 (10), 13–17. https://doi.org/10.1029/2001wr000738, 13-1-.

Crawford, J.W., 1994. The relationship between structure and the hydraulic conductivity of soil. Eur. J. Soil Sci. 45, 493–502.

Dahle, H.K., Celia, M.A., Hassanizadeh, S.M., 2005. Bundle-of-tubes model for calculating dynamic effects in the capillary-pressure-saturation relationship. Transp. Porous Media 58, 5–22. https://doi.org/10.1007/1-4020-3604-3_2.

Diamantopoulos, E., Durner, W., Harter, T., 2016. Prediction of capillary air-liquid interfacial area vs. saturation function from relationship between capillary pressure and water saturation. Adv. Water Resour. 97, 219–223.

Ghanbarian, B., Hunt, A.G., Daigle, H., 2016. Fluid flow in porous media with rough pore-solid interface. Water Resour. Res. 52 (3), 2045–2058.

Giménez, D., Allmaras, R.R., Huggins, D.R., Nater, E.A., 1997. Prediction of the saturated hydraulic conductivity-porosity dependence using fractals. Soil Sci. Soc. Am. J. 61 (5), 1285–1292. https://doi.org/10.2136/sssaj1940.03615995000400c0132x.

Hassanizadeh, S.M., Gray, W.G., 1993. Thermodynamic basis of capillary pressure in porous media. Water Resour. Res. 29 (10), 3389–3405.

Helland, J.O., Skjaeveland, S.M., 2007. Relationship between capillary pressure, saturation, and interfacial area from a model of mixed-wet triangular tubes. Water Resour. Res. 43 (12).

Hirasaki, G.J., 1991. Wettability: fundamentals and surface forces. SPE Formation Eval. 6 (2), 217–226. https://doi.org/10.2118/17367-PA.

Jiang, H., Guo, B., Brusseau, M.L., 2020. Pore-scale modeling of fluid-fluid interfacial area in variably saturated porous media containing microscale surface roughness.. Water Resour. Res. 56. https://doi.org/10.1029/2019WR025876, e2019WR025876.

Kibbey, T.C.G., 2013. The configuration of water on rough natural surfaces: implications for understanding air-water interfacial area, film thickness, and imaging resolution. Water Resour. Res. 49 (8), 4765–4774.

Kim, H., Rao, P.S.C., Annable, M.D., 1997. Determination of effective air-water interfacial area in partially saturated porous media using surfactant adsorption. Water Resour. Res. 33 (12), 2705–2711.

Kim, H., Rao, P.S.C., Annable, M.D., 1999. Gaseous tracer technique for estimating air–water interfacial areas and interface mobility. Soil Sci. Soc. Am. J. 1554–1560.

Kim, T.W., Tokunaga, T.K., Shuman, D.B., Sutton, S.R., Newville, M., Lanzirotti, A., 2012. Thickness measurements of nanoscale brine films on silica surfaces under geologic CO_2 sequestration conditions using synchrotron X-ray fluorescence. Water Resour. Res. 48 (9).

Lampurlanés, J., Cantero-Martínez, C., 2006. Hydraulic conductivity, residue cover and soil surface roughness under different tillage systems in semiarid conditions. Soil Tillage Res. 85 (1–2), 13–26.

Liu, G., Zhang, M., Ridgway, C., Gane, P., 2014. Pore wall rugosity: the role of extended wetting contact line length during spontaneous liquid imbibition in porous media. Colloids Surfaces A: Physicochem. Eng. Aspects 443, 286–295 1016/j.colsurfa.2013.11.033.

Mandelbrot, B.B., 1983. The Fractal Geometry of Nature (Vol. 173). WH freeman, New York.

Oliver, J.P., Huh, C., Mason, S.G., 1980. An experimental study of some effects of solid surface roughness on wetting. Colloids Surfaces 1 (1), 79–104.

Or, D., Tuller, M., 1999. Liquid retention and interfacial area in variably saturated porous media: upscaling from single-pore to sample-scale model. Water Resour. Res. 35 (12), 3591–3605.

Or, D., Tuller, M., 2000. Flow in unsaturated fractured porous media: hydraulic conductivity of rough surfaces. Water Resour. Res. 36 (5), 1165–1177.

Pachepsky, Y.A., Shcherbakov, R.A., Korsunskaya, L.P., 1995. Scaling of soil water retention using a fractal model. Soil Sci. https://doi.org/10.1097/00010694-199502000-00003.

Peng, S., Brusseau, M.L., 2005. Impact of soil texture on air-water interfacial areas in unsaturated sandy porous media. Water Resour. Res. 41 (3).

Peng, S., Brusseau, M.L., 2012. Air-water interfacial area and capillary pressure: porous-medium texture effects and an empirical function. J. Hydrologic Eng. 17 (7), 829–832.

Perfect, E., 1999. Estimating soil mass ffactal dimensions from water retention curves. Geoderma 88, 221–231. https://doi.org/10.1046/j.1365-2389.2001.00418-10.x.

Philip, J.R., 1978. Adsorption and capillary condensation on rough surfaces. J. Phys. Chem. 82 (12), 1379–1385. https://doi.org/10.1021/j100501a012.

Porter, M.L., Schaap, M.G., Wildenschild, D., 2009. Lattice-Boltzmann simulations of the capillary pressure–saturation–interfacial area relationship for porous media. Adv. Water Resour. 32 (11), 1632–1640.

Resurreccion, A.C., Moldrup, P., Tuller, M., Ferré, T.P.A., Kawamoto, K., Komatsu, T., De Jonge, L.W., 2011. Relationship between specific surface area and the dry end of the water retention curve for soils with varying clay and organic carbon contents. Water Resour. Res. 47 (6).

Schaefer, C.E., DiCarlo, D.A., Blunt, M.J., 2000a. Determination of water-oil interfacial area during 3-phase gravity drainage in porous media. J. Colloid Interface Sci. 221 (2), 308–312. https://doi.org/10.1006/jcis.1999.6604.

Schaefer, C.E., Dicarlo, D.A., Blunt, M.J., 2000b. Experimental measurement of air-water interfacial area during gravity drainage and secondary imbibition in porous media. Water Resour. Res. 36 (4), 885–890.

Thompson, M.E., Brown, S.R., 1991. The effect of anisotropic surface roughness on flow and transport in fractures. J. Geophys. Res.: Solid Earth 96 (B13), 21923–21932.

Tokunaga, T.K., 2011. Physicochemical controls on adsorbed water film thickness in unsaturated geological media. Water Resour. Res. (8) 47.

Tokunaga, T.K., Wan, J., 1997. Water film flow along fracture surfaces of porous rock. Water Resour. Res. 33 (6), 1287–1295. https://doi.org/10.1029/97WR00473.

Tokunaga, T.K., Olson, K.R., Wan, J., 2003. Moisture characteristics of Hanford gravels. Vadose Zone J. 2 (3), 322–329.

Toledo, P.G., Novy, R.A., Davis, H.T., Scriven, L.E., 1990. Hydraulic conductivity of porous media at low water content. Soil Sci. Soc. Am. J. 54 (3), 673–679. https://doi.org/10.2136/sssaj1990.03615995005400030007x.

Tuller, M., Or, D., Dudley, L.M., 1999. Adsorption and capillary condensation in porous media: liquid retention and interfacial configurations in angular pores. Water Resour. Res. 35 (7), 1949–1964.

Wenzel, R.N., 1936. Resistance of solid surfaces to wetting by water. Ind. Eng. Chem. 28 (8), 988–994.

Zheng, W., Yu, X., Jin, Y., 2015. Considering surface roughness effects in a triangular pore space model for unsaturated hydraulic conductivity. Vadose Zone J. 14 (7), 1–13. https://doi.org/10.2136/vzj2014.09.0121.

Zhong, H., El Ouni, A., Lin, D., Wang, B., Brusseau, M.L., 2016. The two-phase flow IPTT method for measurement of nonwetting-wetting liquid interfacial areas at higher nonwetting saturations in natural porous media. Water Resour. Res. 52 (7), 5506–5515. https://doi.org/10.1002/2016WR018783.Received.